Tunnel coupling in an ensemble of vertically aligned quantum dots at room temperature

V. V. Nikolaev,* N. S. Averkiev, M. M. Sobolev, I. M. Gadzhiyev, I. O. Bakshaev, M. S. Buyalo, and E. L. Portnoi
A. F. Ioffe Physico-Technical Institute, 26 Politechnicheskaya, St. Petersburg 194021, Russia
(Received 20 July 2009; published 5 November 2009)

We report unambiguous observation of the formation of mixed electronic states in an ensemble of self-assembled vertically aligned quantum dots at room temperature. Three closely spaced layers containing stacked In(Ga)As/GaAs quantum dots are placed in the active region of a two-section semiconductor device, and investigations of the quantum-dot optical properties at different applied electric fields are carried out by means of differential-absorption spectroscopy. A simple semianalytical model, which describes absorption of two layers of coupled quantum dots with an account of the size dispersion, is developed. A comparison between our experimental and theoretical results allows clear attribution of the observed low-photon-energy field-dependent spectral features to the four mixed optical transitions due to the two upper quantum-dot layers. Interpretation of the experimental results reveals an anticrossing of spatially direct and indirect transitions characterized by the energy splitting of approximately 30 meV.

DOI: 10.1103/PhysRevB.80.205304 PACS number(s): 78.67.Hc, 71.35.Cc, 78.55.Cr

I. INTRODUCTION

Constant progress in the research and technology of semiconductor quantum dots (QDs) made possible realization of optoelectronic devices with remarkable room-temperature characteristics.[1–3] In present-day QD devices, mainly three-dimensional confinement of carriers in QDs is exploited and incoherent processes play a major role. However, for prospective quantum-information processing, coherent quantum coupling between the qubits is essential. Vertically aligned semiconductor quantum dots[4–6] (VAQDs) are promising candidates to serve as building blocks for quantum-information processing systems. In such structures with sufficiently thin barriers between the QD layers, the QDs tend to grow one above the other, due to the effect of strain distribution, thus, forming ensembles of stacked QDs, ordered in the vertical direction. In particular, utilizing the tunnel coupling between the localized states in VAQDs (Refs. 7 and 8) was proposed for the realization of optically driven quantum gates.[9]

A significant number of microluminescence experiments on the *individual* stacks of VAQDs at cryogenic temperatures was carried out in the last few years (see review articles in Refs. 10 and 11 and references therein). Particularly, the presence of tunnel coupling in individual stacks of VAQDs was proved unambiguously by observing pronounced anticrossings of the direct and indirect excitons when an electric[7,12,13] or magnetic[14] field was applied. Theoretical calculations of the optical properties of individual VAQDs were also carried out.[15,16]

Despite the substantial progress in the experimental and theoretical research of individual VAQDs, the effect of the quantum coupling on the optical properties of the layered structures containing large number of VAQDs was unclear. Since epitaxially grown dots inherently possess significant size dispersion, the direct observation of the quantum-coupling effects is hampered. The redshift of the inhomogeneously broadened luminescence line of the ensemble of VAQDs with the increase in the number of QD layers or the decrease in the interlayer barrier thickness was interpreted as a signature of the tunnel coupling and subsequent carrier delocalization.[5,6,17] However, blueshifts under similar conditions were also observed[18,19] and explained by the influence of the strain fields and variation in the QD material composition. More conclusive evidence of tunnel coupling in VAQD ensembles were found by means of integrated time-resolved measurements: efficient nonradiative interdot carrier relaxation in ensembles of VAQD stacks at low temperatures was reported.[20,21] Time-resolved study of individual double-dot quantum molecule revealed phonon relaxation between the mixed quantum states.[22]

To our knowledge, there were no consistent theoretical attempts to incorporate inhomogeneous broadening together with quantum coupling into consideration of ensembles of VAQDs. Furthermore, the possibility of quantum coupling between the QDs at room temperature was under question since the coherent tunneling length of an electron is expected to fall sharply with the temperature rise. This issue is difficult to resolve by spectroscopy of individual VAQD stacks since the microluminescence signal is quenched at room temperature due to the thermal escape of carriers from QD quantized levels.

In this paper, we report the room-temperature investigation of an ensemble of VAQDs incorporated into a two-sectional semiconductor device. The architecture of the device allowed us to use Stark-shift differential-absorption (DA) spectroscopy[9,23–26] to obtain a rich variety of well-resolved spectral features, which are dependent on the electrical bias of the absorbing section. A theoretical model of two closely spaced QD layers, which includes inhomogeneous broadening as well as tunnel coupling, is developed allowing a rather straightforward interpretation of the experimental results. The unambiguous presence of the tunnel coupling between the electronic states at room temperature in the ensemble of VAQDs is detected and the basic parameters of VAQDs under consideration are deduced.

II. SAMPLES AND EXPERIMENT

A sample containing VAQDs was grown by means of molecular-beam epitaxy on n^+-doped GaAs (001) substrate.

An n-doped 1.5-μm-thick $Al_{0.35}Ga_{0.75}As$ cladding layer was grown on the substrate, followed by 240 nm of undoped GaAs, then three layers of In(Ga)As QDs were grown, caped with another 240-nm-thick-undoped GaAs layer. It was followed by an upper p-doped 1.5-μm-thick $Al_{0.35}Ga_{0.75}As$ cladding layer and a highly p^+-doped GaAs layer, which formed an upper contact. Thus, the three layers of self-organized In(Ga)As QDs were embedded in the center of the undoped GaAs matrix. The quantum dots were grown by depositing 2.3 monolayers of InAs for each QD layer, and sufficiently thin GaAs barriers were grown in between. The vertical alignment of QDs was observed by means of transmission electron microscopy (TEM); the interdot barrier thickness of approximately 3 nm and the vertical distance between the QD centers of approximately 8 nm were detected. TEM images showed the average lateral size of the lower ("seed") QDs to be approximately 20 nm, and the QD size was increasing along the stack, whereas QD heights varied insignificantly. Such effect of structural asymmetry of nominally symmetric QDs is often observed in this type of VAQDs.[10,11,13] Structurally, our QD complexes are similar to double-QD molecules,[10,11] the major difference being the usage of three layers of QDs. In addition, our sample contains a comparatively dense ensemble of VAQD stacks (approximately 10^{10} stacks per cm^2).

The $Al_{0.35}Ga_{0.75}As$ cladding layers provided refractive-index difference with the center layer, thus, ensuring a light confinement in the center-undoped region containing VAQDs. The doping profile formed pin junction, which allowed applying a varying vertical electric field to the VAQDs by changing electric bias between n and p contacts.

In order to measure absorption of VAQDs at different applied fields, the heterostructure was processed into a single-mode laserlike device [Fig. 1(a)]. The 0.3-μm-deep and 7-μm-wide mesa in a stripe geometry formed a waveguide for the light emitted by QDs. The device was separated into two sections by a shallow (not reaching the QD layers) 25-μm-wide-etched trench. The electrical isolation of the sections was enhanced by ion-beam implantation after etching. Similar design was used for achieving pulsed laser generation in mode-locked regime.[27]

In the studied structure, both sections have equal lengths of $L=1.5$ mm. Our aim was to measure radiation, which was emitted by QDs into waveguide modes, in one of the sections and went through the other section. In order to increase the accuracy of the measurements, optical alignment of the experimental setup was performed in the lasing regime. The lasing was achieved when both sections were pumped by a sufficiently high current of 950 A/cm^2. This was made possible by using three layers of VAQDs; two QD layers provided insufficient gain in order to achieve lasing.[28]

The experimental setup is schematically depicted in Figs. 1(b) and 1(c). The reflectance of the facet from which luminescence is collected (the right-side facet in Fig. 1) was reduced to 6% by antireflection coating. The emission into waveguide modes was excited by pumping one of the sections using the electric current ten times lower than the lasing-threshold current.

On the first stage of the experiment [see Fig. 1(b)], the section closest to the monochromator [the right section in Figs. 1(b) and 1(c)] is excited by electric current, whereas the other section is biased in the opposite direction and the emission spectrum $I_e(\hbar\omega)$ is measured [Fig. 2(a)]. The energy of electroluminescence peak is well below the band gap of

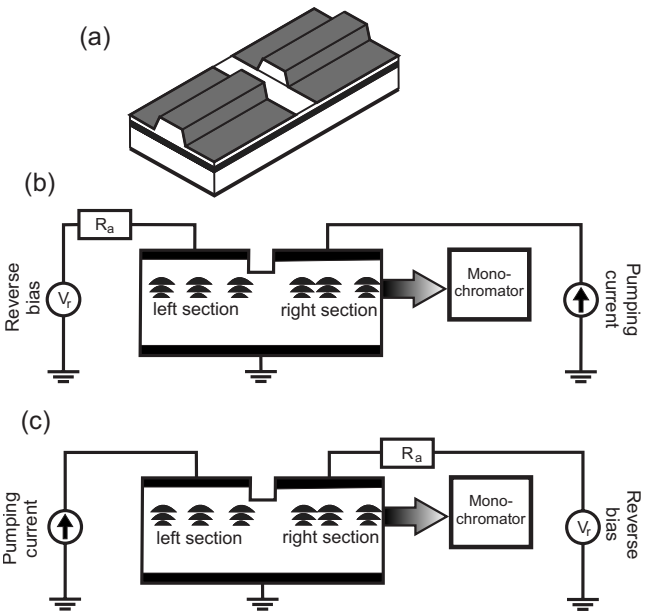

FIG. 1. (a) Schematic representation of the two-sectional semiconductor device. [(b) and (c)] The experimental setup for VAQD absorption measurements: (b) direct detection of electroluminescence spectra and (c) detection of electroluminescence passed through absorbing section.

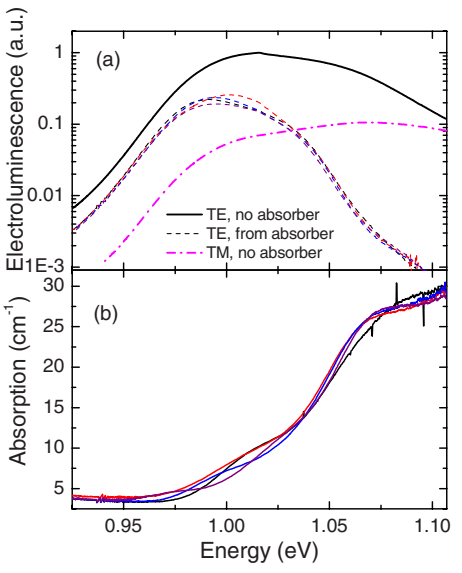

FIG. 2. (Color online) (a) Measured electroluminescence spectra: TE polarized from emission section (solid thick line), TE polarized from the absorbing section at four different applied electric fields varying from 20 to 180 kV/cm (thin dashed lines), and TM-polarized from emission section (thick dash-dotted line). The spectra are normalized to the maximum of the TE-polarized luminescence. (b) Absorption spectra of the three layers of VAQDs at four different applied electric fields derived from TE-polarized electroluminescence spectra (see details in the text).

GaAs matrix and, therefore, the luminescence can be assigned to VAQDs. Because of the electrical separation of the sections, the electroluminescence from the emission section does not depend on the reverse bias of the absorbing section. On the second stage [Fig. 1(c)], the applied voltages on the sections are exchanged, so that the left section is pumped by the same current as the right section was during the first stage. In this case, waveguided radiation from the left section penetrates into the right section almost without loss, then experiences partial absorption by VAQDs in the right section and reaches measuring setup through low-reflectance facet. Field-dependent electroluminescence spectra $I_a(\hbar\omega)$ measured in the described manner are shown in Fig. 2(a) by thin dashed lines. From Fig. 2(a), one can see that electroluminescence from the emission section represents a rather broad line characterized by the full width at half maximum of approximately 80 meV. This is due to substantial inhomogeneous broadening and the overlap of the ground and exited optical transitions. Because of that, the effect of quantum coupling between VAQDs cannot be seen clearly in electroluminescence spectra [Fig. 2(a)].

As Fig. 2(a) shows, TM-polarized electroluminescence is blueshifted with respect to the TE-polarized luminescence peak, and the emission maximum of the TM-polarized luminescence is an order of magnitude lower than the TE-polarized luminescence maximum, which is typical for epitaxially grown QDs with a low aspect ratio.[29] Therefore, one can assume that the lowest QD transitions interact mainly with TE modes of the optical resonator and, hence, we use TE-polarized spectra in our investigations.

Since both sections have the same length and the optical scheme of the experimental setup was not changed, one can assume that the intensity of the emission reaching the absorbing section on the second stage is approximately equal to the emission-section intensity measured on the first stage.[28,29] Therefore, the spectra measured on the first and the second stages are related by a simple expression $I_a(\hbar\omega) = I_e(\hbar\omega)\exp[-L \times \alpha(\hbar\omega)]$, where $\alpha(\hbar\omega)$ is a field-dependent absorption spectrum. This allows obtaining the magnitude of VAQD absorption in absolute values [see Fig. 2(b)] using measured electroluminescence spectra [Fig. 2(a)]. By changing the reverse bias on the absorbing section, we derived the absorption of VAQDs at different applied fields [Figs. 2(b) and 3].

In addition to absorption spectra, DA measurements are performed. A small sinusoidal signal (0.1 V rms, which is approximately 2 kV/cm of the electric-field modulation) at a frequency of 130 Hz is added to the constant voltage applied to the absorbing section in the experimental setup similar to that depicted in Fig. 1(c). The ac part of the luminescence is measured by a lock-in detector. Provided the modulation amplitude is small enough, the obtained ac part of the radiation should be proportional to the derivative of the dc luminescence intensity by the reverse voltage (or, equivalently, by the electric field F applied to VAQDs). The ratio of the demodulated ac signal to the dc spectrum $I_a(\hbar\omega)$ measured previously will give the derivative of the absorption up to a constant factor. The spectra of the absorption differentiated by the applied field are presented in Fig. 4(a); DA spectra of

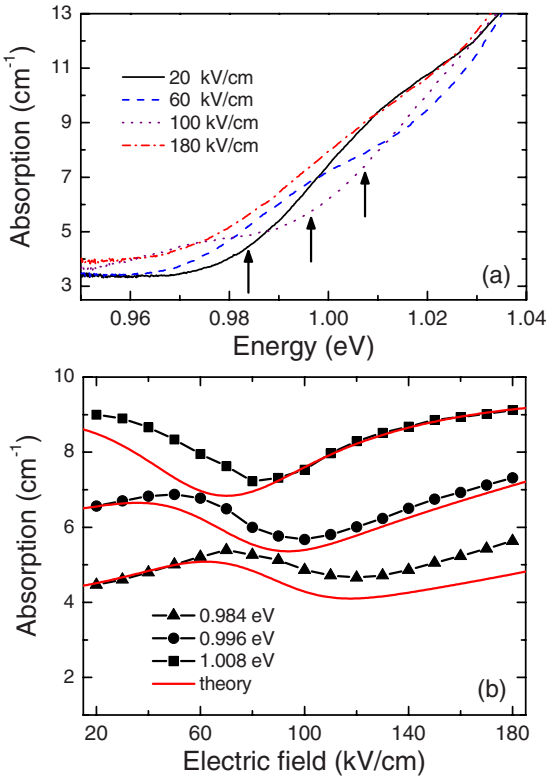

FIG. 3. (Color online) (a) Closeup of the spectra in Fig. 2(b) in the low-photon-energy interval. (b) Measured and calculated absorption at three particular photon energies as a function of applied electric field; the photon-energy values at which the absorption is measured and calculated are indicated in (a) by arrows.

ten layers of uncoupled In(Ga)As QDs (30-nm-interlayer barriers, see Ref. 28 for details) are shown in Fig. 4(b) for the sake of comparison. The absolute values of differential absorption of VAQDs were found by comparing DA magnitudes at particular photon energies and the corresponding derivatives of experimental absorption curves in Fig. 3(b). The spectral range of the reliable DA measurements is limited by the nature of the light source, which is used as a probe. In our case, luminescence of the electrically pumped QDs in one section is used to probe absorption of the QDs in the other section. Sufficiently broad electroluminescence spectrum of QDs [Fig. 2(a)] and high precision of the experimental setup allowed reliable DA measurements in an interval from approximately 0.93 eV to approximately 1.08 eV. At low-photon-energies QDs, on the very tail of QD-size distribution contributed to the emission, hence, the emission intensity at these energies is two orders of magnitude smaller than the emission maximum [Fig. 2(a)].

Differential-absorption method is qualitatively similar to differential *transmission* technique, which was used for the investigation of single QDs,[24] individual VAQDs (Refs. 9 and 25), and multilayered QD ensembles with varying interdot barriers[26] and allowed ultrahigh sensitivity. Ser *et al.* applied differential transmission method to the ensemble of VAQDs and observed a single well-resolved optical transition, which exerted an enhanced Stark shift.[23]

Tuning microluminescence with the applied electric field has been proven to be a powerful method for studying the

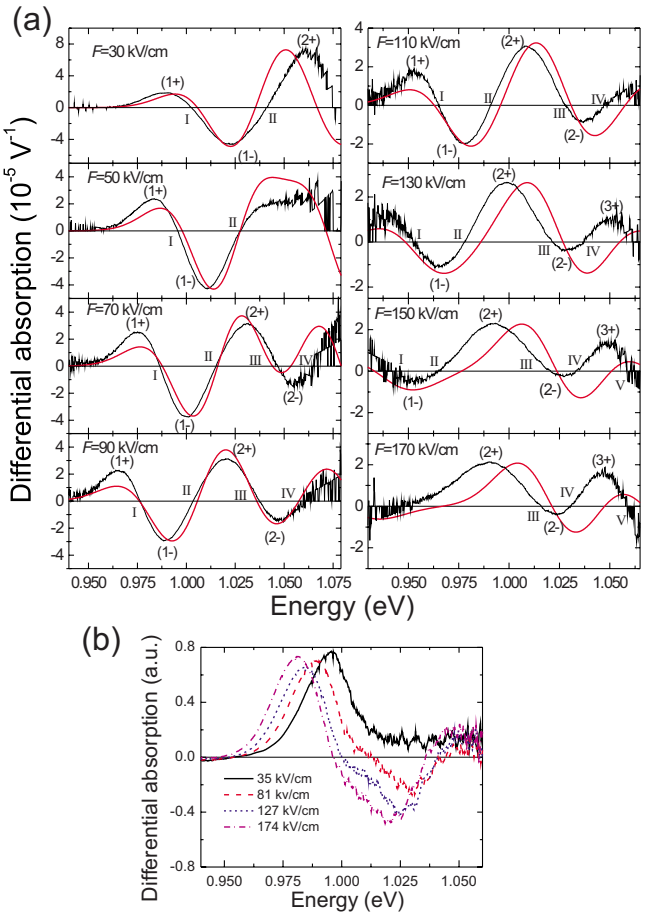

FIG. 4. (Color online) (a) Measured (thin lines) and calculated (thick lines) spectra of the applied-field derivative of the VAQD absorption (i.e., differential absorption) taken at the eight applied fields: 30, 50, 70, 90, 110, 130, 150, and 170 kV/cm. The maxima and minima in the experimental spectra are labeled by (1+), (1−), etc.; the roots of the experimental spectra are labeled by I, II, etc. (b) Measured differential-absorption spectra of ten layers of uncoupled QDs (Ref. 28).

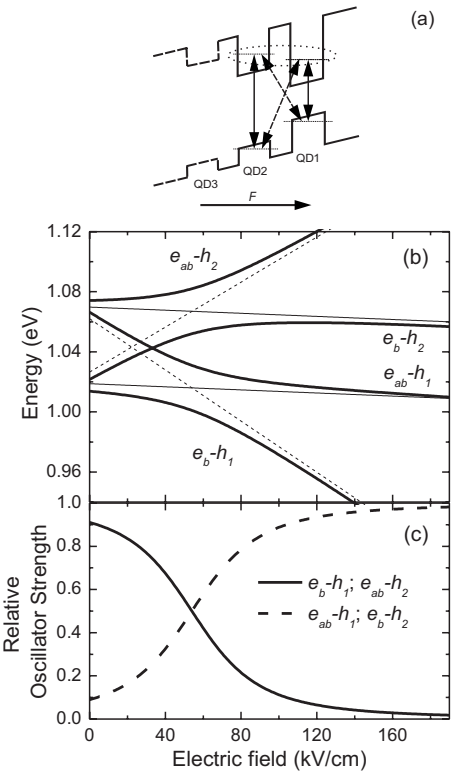

FIG. 5. (a) Schematic band structure of three VAQDs in presence of an applied electric field. The direction of the applied field F, which coincides with the growth direction, is shown. The band profile of the bottom dot with the smallest depth (QD3), which is not included in the theoretical model, is shown by dashed lines. The solid (dashed) arrows indicate intradot (interdot) transitions. Changing the applied field allows the electronic levels to be brought into resonance. (b) Energies of the four optical transitions originating from the ground carrier levels in the system of the two coupled QDs (thick solid curves) as functions of applied field. Energies of the intradot (interdot) transitions are represented by thin solid (dashed) lines. (c) Relative oscillator strengths of the four optical transitions.

quantum-coupling properties of individual VAQDs.[7–9,12,13] Since in our experiments the manipulation of the *absorption* with the applied field is performed, there is no strict limitation on the maximum value of the applied field, which arises in the microluminescence measurements due to luminescence suppression by the carrier escape from QDs. In our case, measurements in a wide range of applied fields (from 20 to 180 kV/cm) were carried out. In addition, one can assume that at high enough fields at room temperature, the occupation of the VAQD carrier levels in the absorbing section is negligible, which simplifies the analysis.

As was pointed above, in the studied structure the lateral size of the QDs in the stack increases in the growth direction, which is the result of strain relaxation during epitaxial growth.[4,6] According to some reported individual-QD-stack investigations, under similar conditions top dots with larger size have smaller ground-transition energies and deeper localized electronic levels than the bottom (smaller) dots.[7,10,30] In this case, electronic levels can be driven into resonance when the electric field is applied along the growth direction[7,13] [see a schematic band diagram in Fig. 5(a)]. We assume that in our structure, the bottom QDs [designated in Fig. 5(a) as QD3] have the larger intradot ground-transition energy and hence smaller carrier localization than the upper QD pair [QD1 and QD2 in Fig. 5(a)]. As long as we consider only the low-energy ("red") part of the spectrum, we can expect that the bottom dots have little impact there. In addition, at large enough applied fields, the levels in the bottom QDs may become strongly delocalized due to its comparatively small depth.

According to these considerations and trying to reduce the number of fitting parameters in order to allow more direct interpretation of the experiment, we consider only two coupled QDs in our theoretical model presented in the next section. These assumptions were subsequently proven by the observation of the electronic resonance when the field is applied along the growth direction and by the absence of any additional spectral features in the red part of experimental spectra, which could be attributed to the third QD layer.

III. THEORY

In this section, a model describing absorption of two coupled QD layers is developed. The electron states in an individual pair of asymmetric VAQDs are treated within the coupled-quantum oscillator approximation.[14,31,32] The single-particle electron Hamiltonian is written in the basis of localized (uncoupled) electron ground states

$$\hat{H}_e = \begin{pmatrix} \varepsilon_{e_1}(F) & \Delta E/2 \\ \Delta E/2 & \varepsilon_{e_2}(F) \end{pmatrix}. \tag{1}$$

Here $\varepsilon_{e_1}(F)[\varepsilon_{e_2}(F)]$ is the field-dependent electron energy in the uncoupled quantum dot QD1 (QD2) and ΔE is the coupling constant (equal to the energy splitting between coupled electron levels at resonance), which is proportional to the tunneling probability. Solving Schrödinger equation with this Hamiltonian gives two mixed eigenstates in the form of linear combinations of the localized states: a symmetric combination and an antisymmetric one. The resulting eigenenergy of the symmetric bonding state ε_e^b is smaller than that of the antisymmetric antibonding state ε_e^{ab}.

We keep only linear and quadratic terms in the electric-field dependence of the uncoupled-QD electron and hole energies

$$\varepsilon_{e_1(h_1)} = \varepsilon^0_{e_1(h_1)} \mp p_{e(h)}F - \beta_{e(h)}F^2,$$

$$\varepsilon_{e_2(h_2)} = \varepsilon^0_{e_2(h_2)} \mp p_{e(h)}F - \beta_{e(h)}F^2 \mp ed \times F, \tag{2}$$

where the upper (lower) signs give expressions for electrons (holes). Here the term $ed \times F$ accounts for the potential drop over the distance d between the two QDs and e is the electron charge. It was implied that the coefficients $p_{e(h)}$ and $\beta_{e(h)}$ are the same for both dots, whereas the zero-field electron (hole) energies $\varepsilon^0_{e_1}$, $\varepsilon^0_{e_2}$ $(\varepsilon^0_{h_1}, \varepsilon^0_{h_2})$ in the two dots have different values in the case of an asymmetric QD pair.

In our experiments, the direction of the applied field is such that it drives the electron levels of asymmetric QDs into resonance, whereas the energy separation between the hole levels is increasing [see Fig. 5(a)]. Because of the larger effective mass, the hole coupling constant is an order of magnitude smaller than that of electrons,[8,13] and it is a good approximation to assume that the holes are localized inside each QD. Therefore, in the system of two coupled QDs there are four optical transitions arising from the ground electron and hole states: two transitions (e_b-h_1 and e_{ab}-h_1) involving the hole in QD1 and one of the mixed electronic states and other two transitions (e_b-h_2 and e_{ab}-h_2) involving the hole localized in the second dot QD2. In case of asymmetric dots with uncoupled hole states, all the four transitions are bright.

Within the single-particle picture, the transition energies have a simple form $E^X_{h_j} = \varepsilon^X_e + \varepsilon_{h_j}$, where the energies of the localized holes ε_{h_1}, ε_{h_2} are given by Eqs. (2) and the energies of the mixed electronic states $\varepsilon^X_e(X=b,ab)$ are obtained by solving the single-particle Schrödinger equation with the Hamiltonian in Eq. (1). These transition energies can be expressed as

$$E^{b(ab)}_{h_1} = E^0_1 - pF - \beta F^2 + \frac{\Delta E}{2}(u \mp \sqrt{u^2+1}),$$

$$E^{b(ab)}_{h_2} = E^0_2 - pF - \beta F^2 - \frac{\Delta E}{2}(u \pm \sqrt{u^2+1}), \tag{3}$$

where $E^0_j = \varepsilon^0_{e_j} + \varepsilon^0_{h_j}$ $(j=1,2)$ is the energy of the ground intradot transition in the jth QD at zero applied field; $p=p_e-p_h$ and $\beta=\beta_e+\beta_h$ are the build-in electric dipole moment and polarizability of the QDs, respectively. In Eqs. (3), a new field-dependent variable $u=(\Delta\varepsilon_e - edF)/\Delta E$ was introduced, where $\Delta\varepsilon_e = \varepsilon^0_{e_2} - \varepsilon^0_{e_1}$ is the difference between electron energies in uncoupled QDs at zero applied field. The value of $\Delta\varepsilon_e$ gives the quantitative measure of asymmetry in the QD pair. The u variable is the energy difference between electron levels of uncoupled QDs reduced to the splitting energy ΔE; it varies linearly with the applied field and turns into zero at resonance. The first three terms in the right-hand side of Eqs. (3) give field dependence of the intradot ground optical transitions in uncoupled QD1 and QD2, whereas the last term accounts for the tunnel coupling.

It should be noted that, although we use the single-particle approximation for the sake of simplicity, the Coulomb effects can be included in the consideration without a major change in formalism. When only one type of carriers is coupled, the Hamiltonian of a neutral exciton can be written in the same form as in Eq. (1), where the coupling parameter ΔE and the zero-field energy of the uncoupled excitons are renormalized by the Coulomb interaction.[33] This would lead to the exciton energy expressions, which are essentially the same as in Eqs. (3).

As the holes are supposed to be localized inside each dot, it can be assumed that the oscillator strength of the optical transition involving a hole in QD1 (QD2) is proportional to the probability to find an electron inside QD1 (QD2). These probabilities are given by the squared modula of the normalized coefficients c_1 and c_2 in the linear-combination representation of the electronic eigenstates

$$|c^b_{1\{2\}}|^2 = |c^{ab}_{2\{1\}}|^2 = \frac{(u \pm \sqrt{u^2+1})^2}{(u \pm \sqrt{u^2+1})^2 + 1}. \tag{4}$$

Here the upper (lower) sign gives the expression of the probability for an electron in the bonding mixed state to be found in QD1 (QD2), and for the antibonding state it is vice versa. According to the Fermi's golden rule, the contribution to absorption of an individual pair of coupled QDs labeled by the index i has the following form $\alpha_i \propto \Sigma_{X=b,ab}[|c^X_1|^2_i \delta(\hbar\omega - E^X_{h1}|_i) + |c^X_2|^2_i \delta(\hbar\omega - E^X_{h2}|_i)]$, where $\hbar\omega$ is the photon energy of the incident light.

To obtain the total absorption of an ensemble of VAQDs, the summation over all the VAQD stacks in the ensemble should be made. To proceed, one has to make certain assumptions about variation in parameters from one individual pair of coupled QDs to another. First we assume that the vertical distance d between the coupled QDs, the coupling constant ΔE, the build-in moment, p and the polarizability β are constant across the ensemble. Second, we assume that the electron-energy difference at zero field (the asymmetry pa-

rameter) $\Delta\varepsilon_e$ is the same for each QD pair in the ensemble. The last assumption can be justified by the experimentally observed significant correlation[34] between the QDs in a stack of vertically aligned QDs. As a consequence of the assumptions made above, the value of u variable will be independent of the QD-pair index i at any applied field. Therefore, the last term in Eqs. (3) and the probabilities in Eq. (4) will not vary across the ensemble. The size dispersion will influence the result through the dependence of the intradot ground-transition energies E_1^0, E_2^0 (or, equivalently, through the dependence of quantized-level energies $\varepsilon_{e_{1,2}}^0$, $\varepsilon_{h_{1,2}}^0$) on the QD-pair index.

A common approach[35] to account for the size dispersion in a QD ensemble is to assign to each QD some size parameter w_i (for instance, the width of the ith QD) and to assume a normal (Gaussian) distribution of this parameter across the ensemble: the number of QDs dN with the value of w_i inside the interval $w_i \in [w, w+dw]$ reduced to the total QD number N_t is given by the formula $dN/N_t=(\delta w)^{-1}\rho([w-\bar{w}]/\delta w)dw$, where the constant $\bar{w}$ is an average value of the size parameter, δw is the standard deviation of the size parameter from the average value, and $\rho(x)=\exp(-x^2/2)/\sqrt{2\pi}$ is the Gaussian function. In addition, it is assumed that the dependence of the electron and hole energies on the size parameter within small deviations from the average value can be approximated by linear functions $\varepsilon_{e(h)}^0|_i=\bar{\varepsilon}_{e(h)}^0+\varepsilon'_{e(h)}\times(w_i-\bar{w})$, where $\bar{\varepsilon}_e^0$, $\bar{\varepsilon}_h^0$ are the average electron and hole energies and ε'_e, ε'_h are constants.

In our case, we use the linear approximation for all the dots in the system in both layers and assume the normal distribution of the size parameter in one of the layers characterized by δw and the average $\bar{w}_1$. From the assumption of the constant difference $\Delta\varepsilon_e$ between the electron levels in each coupled QD pair, it follows that the difference Δw between the QD-size parameters in each coupled pair is constant across the ensemble, and the size-parameter distribution in the other layer is Gaussian with the same standard deviation δw and the average value $\bar{w}_2$ shifted from $\bar{w}_1$ by Δw.

Summation over all coupled QD pairs is substituted by the integration over the size-parameter distribution giving the absorption expression

$$\alpha(\hbar\omega)=\sum_{j=1,2}\sum_{X=b,ab}\alpha_{h_j}^X(\hbar\omega)+\alpha_B, \tag{5}$$

as a sum of a constant background absorption α_B, and the four Gaussian peaks

$$\alpha_{h_j}^X(\hbar\omega)=\frac{\tilde{\alpha}|c_j^X|^2}{\sqrt{2\pi}\delta\varepsilon}\exp\left[-\frac{1}{2}\left(\frac{\hbar\omega-\bar{E}_{h_j}^X(F)}{\delta\varepsilon}\right)^2\right], \tag{6}$$

which originate from optical transitions between localized holes $h=h_1,h_2$ and mixed electronic states $X=b,ab$. In Eq. (6), $\tilde{\alpha}$ is some coefficient, $|c_{1,2}^X|^2$ are given by Eq. (4), and $\delta\varepsilon=|\varepsilon'_e+\varepsilon'_h|\times\delta w$ is the inhomogeneous-broadening energy of each transition. The center energies of the peaks $\bar{E}_{h_j}^X(F)$ are given by Eqs. (3), where instead of the intradot ground-transition energies E_1^0 and E_2^0 of an individual QD pair one should use the average of these energies $\bar{E}_1^0=\bar{\varepsilon}_{e_1}^0+\bar{\varepsilon}_{h_1}^0$ and $\bar{E}_2^0=\bar{\varepsilon}_{e_2}^0+\bar{\varepsilon}_{h_2}^0$. Thus, the field dependence of spectral positions and maximum values of absorption peaks in the ensemble of coupled QDs is analogous to the dependence of the energies and oscillator strengths of the four transitions in an "average" pair of coupled QDs.

The derivative of the absorption by the applied field is given by the following expression:

$$\frac{\partial\alpha(\hbar\omega)}{\partial F}=\sum_{\substack{j=1,2\\X=b,ab}}\left[\frac{\hbar\omega-\bar{E}_{h_j}^X}{\delta\varepsilon}\frac{d\bar{E}_{h_j}^X}{dF}+\frac{d|c_j^X|^2}{dF}\right]\alpha_{h_j}^X(\hbar\omega), \tag{7}$$

where the derivatives $d\bar{E}_{hj}^X/dF$ and $d|c_j^X|^2/dF$ are obtained from Eqs. (3) and (4), respectively. Thus, in the expression of differential absorption [Eq. (7)], each Gaussian peak is multiplied by a function, which is linear with respect to the photon energy.

Therefore, in general, DA contribution of a particular optical transition to the total DA spectrum has both positive and negative parts separated by a root, which can allow resolving adjacent overlapping peaks. In addition, DA contribution is larger for transitions with relatively fast Stark-shift rate and oscillator-strength change. This favors resonantly coupled transitions since such transitions demonstrate faster Stark-shift rates and more preannounced oscillator-strength dependence on the applied field than uncoupled intradot transitions (see details in the following section).

IV. RESULTS AND DISCUSSION

The calculated energies and oscillator strengths of the four lowest optical transitions of an asymmetric VAQD pair are shown in Figs. 5(b) and 5(c) as functions of the applied field F. The following parameters were used: the energy of the QD1 ground transition at zero applied field E_1^0 is 1.026 eV and the respective energy in the second dot is 51 meV larger, i.e., $E_2^0=1.077$ eV; the energy difference between electron levels of the QDs at $F=0$ is taken to be $\Delta\varepsilon_e=43$ meV; the tunnel coupling energy is $\Delta E=30$ meV; and the vertical effective distance between the QDs is $d=8$ nm. The parameters describing the intradot quantum-confined Stark effect (QCSE) are as follows: the build-in dipole moment p is 6.7×10^{-29} C m corresponding to an electron-hole separation of 4.2 Å within a single QD (which coincides with the result of Fry *et al.*[36]) and the polarizability is taken to be $\beta/e=7.5$ nm^2/V. The same values will be used in the following calculations of the VAQD-ensemble absorption for the parameters of the "average" QD pair. From this point of view, these calculations show the field dependence of the center energies of the four broadened absorption peaks [Fig. 5(b)] and their relative maxima [Fig. 5(c)].

As can be seen in Fig. 5(b), the transitions, which involve the same hole, experience anticrossing when the electron states are tuned into resonance. For the chosen set of parameters, the electron resonance happens at the applied field of approximately 54 kV/cm.

In Fig. 2(a), room-temperature electroluminescence spectra from emission- and absorbing sections are presented; ab-

sorption spectra in Fig. 2(b) are derived from luminescence spectra as described above. One can see that different optical transitions cannot be resolved in electroluminescence or absorption spectra, which is due to strong inhomogeneous broadening. The two-step-like shape of the absorption spectra suggests strong influence of the exited QD levels on the total absorption in the higher-energy ("blue") spectral region. The closeup of the red part of the spectra [Fig. 3(a)] reveals an intricate nontrivial variation in the absorption with the field change. The field dependence of the absorption at selected photon energies [Fig. 3(b)] demonstrates strongly nonmonotonic behavior, and the dependence curves vary significantly with the change in spectral position. These effects were absent in the absorption spectra of samples containing uncoupled layers of QDs.[29]

The theoretical simulations of the absorption change shown alongside experimental results in Fig. 3(b) were obtained using Eq. (5), where the following parameters of the VAQD ensemble were used. The inhomogeneous broadening is taken to be $\delta\varepsilon=16$ meV and the maximum absorption value of a single ground-state optical transition $\tilde{\alpha}/(\sqrt{2\pi}\delta\varepsilon)$ is 6 cm^{-1}. The background absorption value $\alpha_{BG}=3.3$ cm^{-1} was derived directly from experimental spectra in Fig. 3(a). The rest of the parameters, which characterize the "average" QD pair, were listed above. One can see a fairly good agreement between experimental results and calculations, despite the fact that the employed theoretical model does not account for the optical transitions associated with the third QD layer and the exited carrier levels. This suggests that the higher-energy transitions have little influence on the red part of the spectrum.

Strong overlapping of the inhomogeneously broadened optical transitions hampers direct analysis of the absorption spectra. This problem can be largely circumvented by using differential-absorption spectroscopy described in Sec. II. The measured DA spectra presented in Fig. 4(a) reveal a rich variety of field-dependent spectral features. These spectra are qualitatively and quantitatively different from DA spectra of uncoupled QDs[28] shown in Fig. 4(b). In case of uncoupled QDs, only one peak and one well-resolved root are observed in the spectra in the wide interval of applied fields. These spectral features demonstrate slow redshift with the rate of approximately 0.5 meV per 10 kV/cm, which is a typical Stark shift of In(Ga)As quantum dots.[36] On the contrary, up to five roots appear in the DA spectra of VAQDs at different applied fields; their energy positions are shown in Fig. 6(a). Three peaks and two dips are observed in experiment; their spectral positions and the values of extrema are plotted in Figs. 6(b) and 7, respectively. The spectral shifts in Fig. 6 vary substantially with the applied field, ranging from a slow blueshift of (2+) maximum at low applied fields to fast redshifts of the low-energy spectral features on the order of 10 meV per 10 kV/cm at high applied fields.

The results of the theoretical modeling of DA spectra [Eq. (7)] are shown in Figs. 4, 6, and 7 alongside experiment. The values of the parameters listed above were obtained by fitting theoretical calculations to DA experimental data. It was found that despite a significant number of parameters, only two major reduced values define qualitative characteristics of the DA dependence on electric field. These parameters are

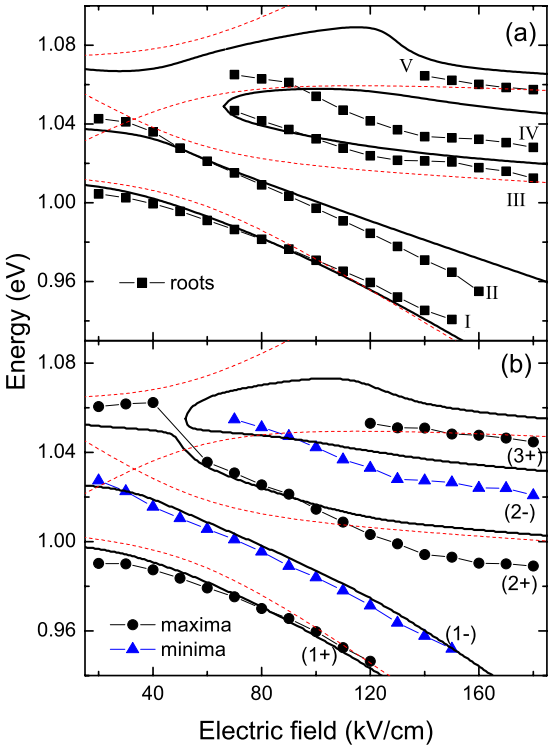

FIG. 6. (Color online) Spectral positions of the (a) roots (squares) and (b) maxima (circles) and minima (triangles) of the differential-absorption spectra (see Fig. 4) as functions of applied electric field. Theoretical calculations of these values are shown by thick solid lines. The calculated average transition energies [Fig. 5(b)] are shown by thin dashed lines in the both panels; in (b) the transition energies are shifted by 20 meV downward for the sake of convenient comparison.

the reduced tunnel coupling parameter $\Delta E/\delta\varepsilon$ and the reduced asymmetry parameter $(\bar{E}_2^0-\bar{E}_1^0)/\delta\varepsilon$. When these two parameters are fixed, the role of the rest of the parameters ($\delta\varepsilon$, d, $\tilde{\alpha}$, $\Delta\varepsilon_e$, and $\bar{E}_0^{(1)}$) is limited to axes scaling or shifting the dependence curves along the axes. The intradot QCSE parameters p and β have significant influence only on the extrema values (Fig. 7) at high applied fields.

One can see that there is a good qualitative and, in some particular field intervals, quantitative agreement between the experimental and theoretical results. The calculated and measured DA spectra are qualitatively similar, demonstrating the same number of roots and extrema in the spectral interval under investigation, and the character of the field dependence of the experimental spectral features coincides with theoretical findings.

In order to establish the origins of the observed spectral features, we decompose theoretical spectra into the four components, each due to a particular optical transition (Figs. 8 and 9). As can be seen from Eq. (7), the contribution of a *single* inhomogeneously broadened transition to the DA spectrum has a form of a Gaussian peak multiplied by a linear function of photon energy. If the Stark shift of the transition is nonzero $d\bar{E}_{h_j}^X/dF\neq 0$, the DA spectrum of a particular transition has a single root: one positive maximum and one negative minimum (see Figs. 8 and 9). The photon

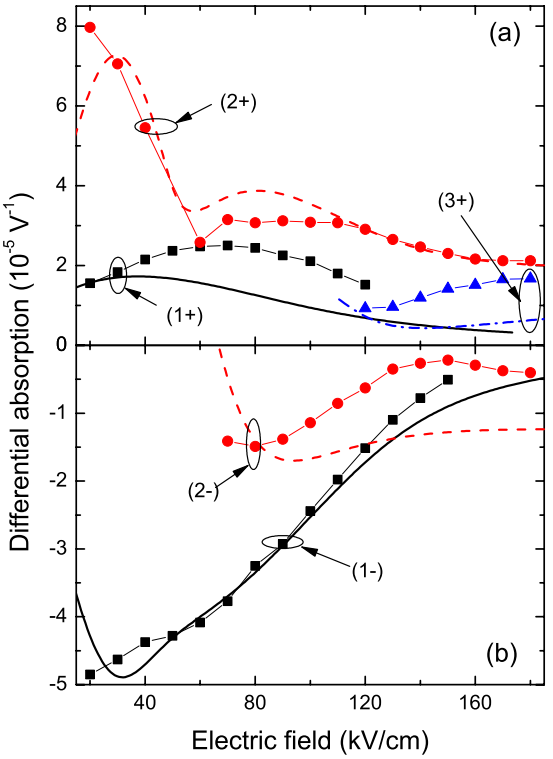

FIG. 7. (Color online) Measured and calculated (a) maxima and (b) minima of the differential-absorption spectra as functions of the applied electric field. Top panel (a) shows measured magnitudes of (1+) (squares), (2+) (circles), and (3+) (triangles) maxima; the related calculation results are given by solid, dashed, and dash-dotted lines, respectively. The bottom panel (b) shows measured magnitudes of (1−) (squares) and (2−) (circles) minima; the related calculation results are given by solid and dashed lines, respectively.

energy of the maximum is higher (lower) than that of the minimum in case of the blue(red)shift of the optical transition with an increase in the field. If the variation in the oscillator strength can be neglected [$d|c_j^X|^2/dF=0$ in Eq. (7)], the root of the DA spectrum coincides with the center energy of the broadened absorption peak, and the spectrum form is antisymmetric with respect to its root. The absolute values of the maxima and minima in this case are the same and proportional to the shift rate of this particular transition. When the transition experiences the increase (decrease) in the oscillator strength [Fig. 5(c)], the value of the DA maximum becomes larger (smaller) than the absolute value of the minimum and the root position deviates from the center energy of the absorption peak.

Let us consider the decomposition of the DA spectrum for the applied field of $F=30$ kV/cm [Fig. 8(a)]. As can be seen in Figs. 5(b) and 5(c), the lowest e_b-h_1 transition demonstrates a redshift and the decrease in the oscillator strength with the increase in F. Therefore, this transition contributes a maximum in the low-energy region to the total DA spectra, and the absolute value of the e_b-h_1 DA minimum is much larger than that of the maximum. The e_{ab}-h_1 transition is as well redshifting and, as a consequence, its DA maximum appears at lower energies than its minimum. But, unlike e_b-h_1 transition, the oscillator strength of this transition is

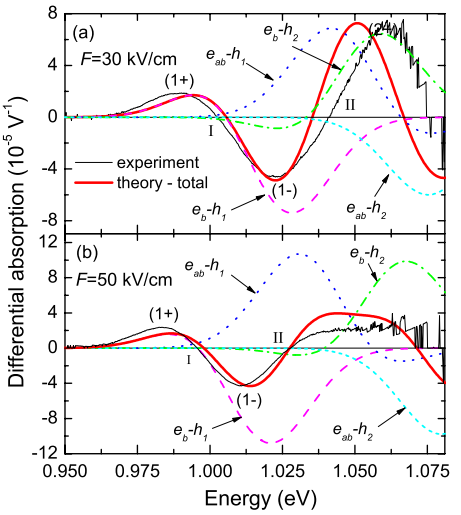

FIG. 8. (Color online) Differential-absorption spectra at the applied electric fields of (a) $F=30$ kV/cm and (b) $F=50$ kV/cm. The experimental spectra are shown by thin solid lines, the total theoretical spectra are shown by thick solid lines, and calculated contributions from the four optical transitions are represented by dashed (e_b-h_1), dotted (e_{ab}-h_1), dash-dotted (e_b-h_2), and short-dashed (e_{ab}-h_2) lines.

increasing [Fig. 5(c)], which gives a pronounced peak and a modest dip in DA spectra. The e_b-h_2 transition, which blueshifts at this particular applied field, has its maximum at larger energies than the minimum, with the maximum-to-minimum ratio larger than unity due to the gain in the oscillator strength. The absorption derivative of e_{ab}-h_2 transition is negative in the spectral interval under consideration, which is due to the fact that at this particular field the decrease in the oscillator strength has significantly larger effect on the absorption change in this transition than its weak blueshift [Figs. 5(b) and 5(c)].

Now the experimental results can be interpreted. As can be seen in Fig. 6, the measured spectral positions of the root I and the (1+) maximum demonstrate weak redshift at low F

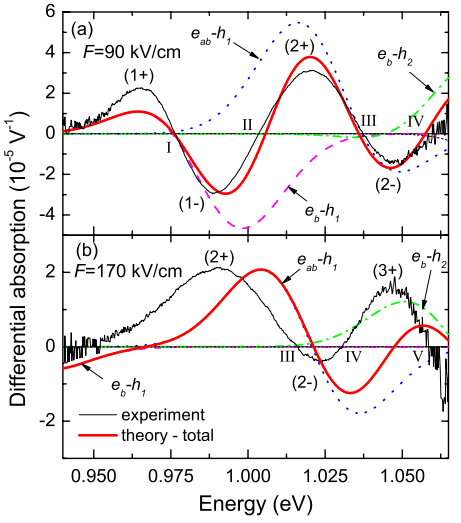

FIG. 9. (Color online) Same as Fig. 8, but for the applied fields of (a) $F=90$ kV/cm and (b) $F=170$ kV/cm.

with the substantial increase in the shift rate at higher applied fields. From examining the decomposition of the total calculated spectra into components in Figs. 8 and 9, one can see that the calculated spectral features, which correspond to the measured root I and the (1+) maximum, are due to the contribution of the e_b-h_1 transition. The experimentally observed increase in the shift rate can be explained by the mixed nature of the e_b-h_1 transition, which transforms from a predominantly intradot character at low F to interdot character at high F. This is also confirmed by the observed decrease of the (1+) maximum and (1−) minimum values (Fig. 7) with an increase in F, which is due to the fall of the e_b-h_1 oscillator strength. At high applied fields, the energy of the e_b-h_1 mixed transition decreases rapidly with the field increasing (Fig. 5), which is manifested in experiment by the (1+), (1−) extrema, and root I eventually vanishing from the spectra at $F>150$ kV/cm [see Figs. 4 and 9(b)]. The fact that these spectral features with the interdot character of the Stark shift are observable in experiment at high applied fields up to 150 kV/cm proves the presence of the strong quantum coupling between the dots characterized by large enough splitting (30 meV) in the system under consideration.

Figure 7(a) shows that the (2+) maximum has the largest value at low applied fields. With the increase in F, there is a sharp decline in the peak magnitude accompanied with a weak blueshift of its spectral position [Fig. 6(b)]. At the applied field of $F\approx 50$ kV/cm, the (2+) peak vanishes, leaving a relatively flat plate in the DA spectrum (see Figs. 4 and 8; note that the y-axis scale in Fig. 4 for $F=30$ kV/cm is different from that of $F=50$ kV/cm). This effect can be explained using our theoretical model. At low applied fields [see Fig. 8(a)], the value of the (2+) peak is enhanced by the positive DA contributions of the two optical transitions: the redshifting e_{ab}-h_1 transition and a blueshifting e_b-h_2 transition. As can bee seen in Fig. 5(b), the dispersion curves of these transitions intersect at $F\approx 30$ kV/cm, and the oscillator strengths of both transitions gain value with the field increase. Both of these developments contribute to the formation of a dominant (2+) peak in the DA spectrum. As the applied field increases further [see Fig. 8(b) for $F=50$ kV/cm], energy distance between the DA maxima of the e_{ab}-h_1 and e_b-h_2 transitions grows, which is due to the fact that the center energies of these transitions shift in opposite directions. This causes elimination of the strong maximum and formation of the flat plate [Fig. 8(b)].

As the applied field exceeds $F\approx 50$ kV/cm, the (2+) peak reappears from the broad flat region (see Fig. 4). With the further increase in F, the (2+) peak steadily moves to lower energies and the shift rate becomes slower with the increase in the field [Fig. 6(b)]. The value of the (2+) maximum in this region of applied fields experience comparatively moderate variation [Fig. 7(a)]. This behavior can be explained by spectral decomposition presented in Fig. 9. By analyzing it, one can conclude that for the fields exceeding 50 kV/cm, the (2+) maximum (as well as root III) is largely due to the redshifting e_{ab}-h_1 transition influenced to some extent by the overlap with the lower e_b-h_1 transition and the higher e_b-h_2 transition. With the increase in F, the e_{ab}-h_1 mixed transition demonstrates changeover from an interdot to the intradot character, which is manifested in the decrease in the spectral shift rate and saturation of the oscillator strength at high applied fields [Fig. 5(b) and 5(c)]. This development is experimentally observed in the decrease in the Stark-shift rate of the (2+) peak and the root III. Furthermore, the moderate variation in the peak (2+) maximum at high F [Fig. 7(a)] is well explained by the gradual turning of mixed e_{ab}-h_1 transition into an almost intradot (QD1) transition at high fields. The observed anticrossing of the e_b-h_1 and e_{ab}-h_1 transitions is in accordance with the reported investigations of individual VAQD stacks.[7,22]

The minor (2−) dip, which appears in experimental spectra at applied fields of $F\geq 70$ kV/cm, is, according to decomposition in Fig. 9, due to the negative contribution of e_{ab}-h_1 transition influenced by the overlap with the higher e_b-h_2 transition. The (3+) peak visible in experiments at high applied fields of $F\geq 120$ kV/cm is associated with the positive DA contribution of the redshifting e_b-h_2 transition [Fig. 9(b)].

At large applied fields of $F\geq 150$ kV/cm, the two peaks (2+), (3+), one dip (2−) and three roots III, IV, and V are present in the experimental spectra; all of which can be attributed to the two mixed transitions e_{ab}-h_1 and e_b-h_2. These are the only transitions which remain in the spectral interval under consideration at high applied fields [see Fig. 5(b)]. The experimental spectral features observed at high applied fields demonstrate comparatively slow redshift (Fig. 6), which is consistent with the transformation of e_{ab}-h_1 and e_b-h_2 mixed transitions into intradot transitions associated with QD1 and QD2, respectively.

Thus, we have shown that the whole wealth of experimentally observed spectral features in a wide range of applied fields fits the picture based on the four inhomogeneously broadened mixed transitions. Nevertheless, one can see that, at large applied fields ($F\geq 130$ kV/cm), the quantitative agreement between theory and experiment is lost [Figs. 4 and 9(b)] with the appearance of a 10–15 meV energetic shift between calculated and measured spectra. There can be several possible reasons for this discrepancy. First, the nonresonant penetration of the electronic wave functions into adjacent QDs and/or into barriers can take place at high applied fields which may lower the electron energy. Second, the decrease in the electron-hole overlap in a single QD at high fields may cause an additional decrease in the oscillator strength and, thus, influence the differential-absorption spectra. These effects were unaccounted by our simplified theoretical approach. Additionally, the VAQD system may deviate from simplified coupled-quantum-oscillator description, which uses constant coupling factor, when it is driven far from resonance.

In Fig. 7, one can see that there is a good quantitative agreement between the experimental and calculated values of the largest (2+) and (1−) extrema, with the exception for very low applied fields ($F<30$ kV/cm). This discrepancy can be explained by the influence of the exited levels and the optical transitions in the third QD, which may play important role at low applied fields in the blue part of the spectrum. For the values of the minor local extrema, namely, (1+), (3+), and (2−), there is only qualitative but not quantitative match between the measured and calculated field dependence. This may be due to the deviation of the QD line shape from the

Gaussian symmetric form, which takes place if the dependence of the energies of QD quantized levels on QD size is strongly nonlinear. The distortion of the distribution shape will mostly affect the "wings" of the distribution. As the minor local extrema in the DA spectra are mainly due to the states distant from the distribution center, they may be strongly influenced by the line-shape distortion.

In conclusion, we have demonstrated electron tunnel coupling in a system containing three layers of vertically aligned quantum dots at room temperature. A theoretical model of a double-layer QD structure, which takes into account tunnel coupling and inhomogeneous broadening, has been developed and allowed clear attribution of the observed field-dependent spectral features in the low-photon-energy interval to the four mixed optical transitions due to the two upper QD layers. Our results represent an unambiguous observation of the quantum coupling in the disordered ensembles of epitaxially grown VAQDs at room temperature. These results suggest a possibility of utilizing coherent properties of coupled QDs in optoelectronic devices for room-temperature operation.

ACKNOWLEDGMENTS

The authors thank A. P. Vasiliev and V. S. Mikhrin for the growth of the sample structures and V. N. Nevedomskiy for TEM images. V.V.N. acknowledges financial support from NATO Reintegration Grant. This work was supported by the Russian Foundation for Basic Research.

*valentin.nikolaev@mail.ioffe.ru

[1] D. Bimberg, M. Grundmann, F. Heinrichsdorff, N. N. Ledentsov, V. M. Ustinov, A. E. Zhukov, A. R. Kovsh, M. V. Maximov, Y. M. Shernyakov, B. V. Volovik, A. F. Tsatsul'nikov, P. S. Kop'ev, and Zh. I. Alferov, Thin Solid Films **367**, 235 (2000).

[2] H. Liu, D. Childs, T. Badcock, K. Groom, I. Sellers, M. Hopkinson, R. Hogg, D. Robbins, D. Mowbray, and M. Skolnick, IEEE Photonics Technol. Lett. **17**, 1139 (2005).

[3] S. S. Mikhrin *et al.*, Semicond. Sci. Technol. **20**, 340 (2005).

[4] Q. Xie, A. Madhukar, P. Chen, and N. P. Kobayashi, Phys. Rev. Lett. **75**, 2542 (1995).

[5] G. S. Solomon, J. A. Trezza, A. F. Marshall, and J. S. Harris, Jr., Phys. Rev. Lett. **76**, 952 (1996).

[6] N. N. Ledentsov *et al.*, Phys. Rev. B **54**, 8743 (1996).

[7] H. J. Krenner, M. Sabathil, E. C. Clark, A. Kress, D. Schuh, M. Bichler, G. Abstreiter, and J. J. Finley, Phys. Rev. Lett. **94**, 057402 (2005).

[8] E. A. Stinaff, M. Scheibner, A. S. Bracker, I. V. Ponomarev, V. L. Korenev, M. E. Ware, M. F. Doty, T. L. Reinecke, and D. Gammon, Science **311**, 636 (2006).

[9] L. Robledo, J. Elzerman, G. Jundt, M. Atatüre, A. Högele, S. Fält, and A. Imamoglu, Science **320**, 772 (2008).

[10] H. J. Krenner, S. Stufler, M. Sabathil, E. C. Clark, P. Ester, M. Bichler, G. Abstreiter, J. J. Finley, and A. Zrenner, New J. Phys. **7**, 184 (2005).

[11] L. Wang, A. Rastelli, S. Kiravittaya, M. Benyoucef, and O. G. Schmidt, Adv. Mater. **21**, 2601 (2009).

[12] G. Ortner, M. Bayer, Y. Lyanda-Geller, T. L. Reinecke, A. Kress, J. P. Reithmaier, and A. Forchel, Phys. Rev. Lett. **94**, 157401 (2005).

[13] A. S. Bracker, M. Scheibner, M. F. Doty, E. A. Stinaff, I. V. Ponomarev, J. C. Kim, L. J. Whitman, T. L. Reinecke, and D. Gammon, Appl. Phys. Lett. **89**, 233110 (2006).

[14] G. Ortner *et al.*, Phys. Rev. B **71**, 125335 (2005).

[15] Y. B. Lyanda-Geller, T. L. Reinecke, and M. Bayer, Phys. Rev. B **69**, 161308(R) (2004).

[16] B. Szafran, E. Barczyk, F. M. Peeters, and S. Bednarek, Phys. Rev. B **77**, 115441 (2008).

[17] S. Fafard, M. Spanner, J. P. McCaffrey, and Z. R. Wasilewski, Appl. Phys. Lett. **76**, 2268 (2000).

[18] H. Heidemeyer, S. Kiravittaya, C. Müller, N. Y. Jin-Phillipp, and O. G. Schmidt, Appl. Phys. Lett. **80**, 1544 (2002).

[19] S. Taddei, M. Colocci, A. Vinattieri, F. Bogani, S. Franchi, P. Frigeri, L. Lazzarini, and G. Salviati, Phys. Rev. B **62**, 10220 (2000).

[20] T. Nakaoka, J. Tatebayashi, Y. Arakawa, and T. Saito, J. Appl. Phys. **96**, 150 (2004).

[21] J. S. Yim, Y. D. Jang, D. Lee, H. G. Lee, and S. K. Noh, J. Appl. Phys. **98**, 023518 (2005).

[22] T. Nakaoka, E. C. Clark, H. J. Krenner, M. Sabathil, M. Bichler, Y. Arakawa, G. Abstreiter, and J. J. Finley, Phys. Rev. B **74**, 121305(R) (2006).

[23] J. Ser, Y. Lee, J. Kim, and J. Oh, Jpn. J. Appl. Phys. **39**, L518 (2000).

[24] B. Alén, F. Bickel, K. Karrai, R. J. Warburton, and P. M. Petroff, Appl. Phys. Lett. **83**, 2235 (2003).

[25] S. Fält, M. Atatüre, H. E. Türeci, Y. Zhao, A. Badolato, and A. Imamoglu, Phys. Rev. Lett. **100**, 106401 (2008).

[26] K. Chuang, C. Chen, T. Tzeng, D. J. Feng, and T. Lay, J. Cryst. Growth **311**, 1767 (2009).

[27] A. Gubenko, D. Livshits, I. Krestnikov, A. K. S. Mikhrin, A. Kovsh, N. Ledentsov, A. Zhukov, and E. Portnoi, Electron. Lett. **41**, 1124 (2005).

[28] M. M. Sobolev, I. M. Gadzhiyev, I. O. Bakshaev, V. S. Mikhrin, V. N. Nevedomskiy, M. S. Buyalo, Y. M. Zadiranov, and E. L. Portnoi, Semiconductors **43**, 490 (2009).

[29] E. L. Portnoi, I. M. Gadzhiev, A. E. Gubenko, M. M. Sobolev, A. R. Kovsh, and I. O. Bakshaev, Tech. Phys. Lett. **33**, 686 (2007).

[30] M. Scheibner, M. Yakes, A. S. Bracker, I. V. Ponomarev, M. F. Doty, C. S. Hellberg, L. J. Whitman, T. L. Reinecke, and D. Gammon, Nat. Phys. **4**, 291 (2008).

[31] M. F. Doty, M. Scheibner, A. S. Bracker, I. V. Ponomarev, T. L. Reinecke, and D. Gammon, Phys. Rev. B **78**, 115316 (2008).

[32] M. Bayer, P. Hawrylak, S. F. K. Hinzer, M. Korkusinski, Z. R. Wasilewski, O. Stern, and A. Forchel, Science **291**, 451 (2001).

[33] See supporting online material for E. A. Stinaff, M. Scheibner, A. S. Bracker, I. V. Ponomarev, V. L. Korenev, M. E. Ware, M. F. Doty, T. L. Reinecke, and D. Gammon, Ref. 8.

[34] Z. R. Wasilewski, S. Fafard, and J. P. McCaffrey, J. Cryst. Growth **201-202**, 1131 (1999).

[35] L. V. Asryan and R. A. Suris, Semicond. Sci. Technol. **11**, 554 (1996).

[36] P. W. Fry *et al.*, Phys. Rev. Lett. **84**, 733 (2000).